On the calculation of cumulative strain around full-flow penetrometers in steady-state conditions

Ashraf S. Osman[1] and Mark F Randolph[2]

Abstract

An approximate solution for the effects of high strain rates, and gradual strength degradation, on the penetration resistance of penetrometers can be obtained by combining the strain-path method with the classical upper bound theorem. The stream path calculations require the integration of the material constitutive equation along the streamlines. Unless the geometry is simple so that the integration can be evaluated analytically, numerical procedures are required to back-track streamlines. The strain at any location is calculated by finding the streamline that passes through the given point and integrating the strain rate along that streamline from its inlet boundary. Thus, the calculations can be complicated and errors can be accumulated during the calculation procedure.

This paper presents an efficient approach for evaluating cumulative strains around penetrometers without the need to back-track individual streamlines. In this approach the strain components are treated as field variables. The global solution is obtained using the Streamline Upwind Petrov–Galerkin (SUPG) method. The new method together with an Eulerian-based finite element formulation were used to study the cone penetration test (CPT) and evaluate the effect of strain softening on the cone resistance.

[1] Lecturer, School of Engineering, Durham University, South Road, Durham DH1 3LE, UK; Tel: +44 191 334 4245; Fax: +44 191 334 2390; E-mail: ashraf.osman@durham.ac.uk

[2] Professor of Civil Engineering, Centre for Offshore Foundation Systems, University of Western Australia, Perth, WA6009, Australia, Tel:+61 8 6488 3075; Fax: +61 86488 1044 ; E-mail: mark.randolph@uwa.edu.au

Introduction

In several geotechnical problems such as full-flow (T-bar and ball) penetrometers, cone penetration test, and pile installation, the onset and growth of damage in the surrounding geomaterial depends on the rates of deformation and the magnitude of strain (or material structure). In such applications, modelling the deformation and stress histories of soil particles as they move during the penetration process is important.

A major development of modelling deep penetration problems was provided by Levadoux and Baligh [1] and Baligh [2] who introduced the strain-path method as an approximate analytical produce for estimating strains and stresses around penetrometers. Using this approach, the quasi-static penetration problem is modelled as a steady flow of soil past a stationary penetrometer. Soil strains are estimated from an approximate velocity field and stresses are obtained by integrating the strain paths of the soil element. This method has been applied to cone penetration [3-6].

Einav and Randolph [7] calculated the penetration resistance of T-bar and ball penetrometers by combining the strain-path method with the upper bound theorem, equating the external work to the internal plastic work. The strain paths were obtained by generating streamlines from the velocity field obtained from an optimal upper bound mechanism. A similar approach was adopted by Klar and Osman [8], but instead of using a conventional upper bound mechanism they employed mechanisms derived from elastic fields using the Airy stress function (or Airy potential). Therefore, their solution does not require any special treatment of discontinuity lines (which exist for the cylindrical T-bar geometry, though not for the axisymmetric ball).

In the stream path methods, the constitutive equations must be integrated along the streamlines. Unless the geometry is simple so that the integration can be evaluated analytically, numerical procedures are required to identify streamlines and hence incremental plastic work throughout the soil regime. The strain at any location is calculated by finding the streamline which passes through that point and integrating the strain rate along that streamline from its inlet boundary. Klar and Pinkert [9] developed a numerical procedure for evaluating strains where they are treated as spatially continuous parameters. In a finite difference grid, the strain at each point of the grid is evaluated from the strains and the

velocities of two neighbouring points although the calculations are not straightforward as they have to be carried out in certain topological sequences starting from the inlet boundary.

The finite element method has been implemented successfully to model history-dependent geotechnical problems [10]. The formulations are based either on small deformations or using updated Lagrangian theory. In the Lagrangian formulation, an initial value ordinary differential equation for material evaluation at each Gauss point is solved by a time incremental scheme. Lagrangian formulations have been applied to many geotechnical applications and have proven to be robust and algorithmically easier to implement.

However, when the material deforms severely, elements becomes similarly distorted since mesh points are attached to material points in the Lagrangian description. The approximation accuracy of the elements then deteriorates, particularly for higher order elements, causing numerical instability [11]. This is commonly observed when modelling the penetration process, which exhibits very large deformations. Arbitrary Lagrangian–Eulerian (ALE) formulations are used in these problems [12]. In the ALE formulations, the mesh motion does not necessarily coincide with the material deformation so that severe element distortion can be eliminated. However, this requires an effective algorithm for updating the mesh since numerical errors may develop and propagate over time during the analysis. This constitutes a hurdle in developing an effective implementation of the ALE description.

The use of Eulerian reference frames is advantageous in analysing steady-state conditions. The solution can be obtained without following the process through its transient phase. This can lead to computational efficiency, provided that information concerning the transient state is not required, and avoids difficulties that may arise if distortion becomes large. In such computations, the nodal points do not correspond to material points but rather the material passes through a spatially fixed mesh. Therefore, in an Eulerian frame the time derivative terms are transformed to spatial gradient terms. It is therefore necessary to develop supplement methods for evaluating the strain or other quantities that evolve with the flow.

Two common techniques are used in the Eulerian formulation to evaluate strains: mixed formulation and streamline method. In a mixed formulation, the partial differential equations describing material evolution include convection terms, which may result in non-physical

oscillations in the solution. The most common method used to handle these convection-dominated problems is the streamline upwind Petrov–Galerkin (SUPG) method [13–16]. In the SUPG method, the weighting function is the interpolation terms plus an additional mesh-dependent term. The mixed formulation could be computationally expensive because of the large number of field variables that need to be determined. For example, the plane-strain formulation of Qin and Michaleris [17] for an elasto-plastic material requires finding solutions for 11 field variables at each node in a four-node quadrilateral element mesh.

In the streamline method, a sequential iterative approach is used, where the velocity field is solved first from the governing equation. Then, streamlines are computed from the velocity field along which the constitutive equation is integrated to obtain the stress and strain. Agrawal and Dawson [18] obtained strain by integrating the material derivative of the deformation gradient tensor over the domain. Large strain measures such as large Green Strain is then used to calculate the strain from the deformation gradient **F**. The Galerkin formulation was used to obtain the weighted residual. However, because of the convection term, the Galerkin formulation can lead to numerical instability [19]. Furthermore, Agrawal and Dawson's formulation yields a matrix equation for **F** that is partitioned in such a way that the components of **F** are not all coupled in the case of two and three dimensional flow. This can lead to non-zero volumetric strain if applied directly to incompressible materials. In geotechnical applications, penetrometer testing in clay under undrained conditions is associated with zero volume change. Therefore, a robust numerical procedure for evaluating strain from a velocity field in an incompressible material is required.

This paper presents an efficient technique for calculating cumulative strains around moving penetrometers for steady-state conditions. The new technique can be either used in the strain path method where the velocity field is assumed or it can be integrated into the finite element method where the velocity is treated as a field variable. The authors will present algorithms for the finite element analysis of a penetrometer advancing in an elasto-plastic material. The proposed numerical procedures can be used to give insight into the flow mechanisms around penetrometers and to provide correlation between the penetration resistance and the material properties. Although, in this paper the authors demonstrate this approach for a von Mises perfectly plastic material, it is relatively straightforward to apply to more advanced constitutive models.

Governing equation for strain evaluation

In a flow field described by an Eulerian reference frame, the material derivative of the strain tensor $\boldsymbol{\varepsilon}$ can be defined as:

$$\dot{\boldsymbol{\varepsilon}} = \frac{D\boldsymbol{\varepsilon}}{Dt} = \frac{\partial \boldsymbol{\varepsilon}}{\partial t} + \mathbf{v}.\nabla\boldsymbol{\varepsilon} \tag{1}$$

where $\mathbf{v}$ is the velocity vector.

If steady-state conditions are assumed then the partial derivative with time (the local time derivative) is eliminated, hence

$$\dot{\boldsymbol{\varepsilon}} = \mathbf{v}.\nabla\boldsymbol{\varepsilon} \tag{2}$$

A weighted residual W is formed by integrating equation (2) with a set function $\mathbf{N^P}$ over the domain. The residual is then required to vanish:

$$W = \int_{\Omega} \mathbf{N^P}(\mathbf{v}.\nabla\boldsymbol{\varepsilon} - \dot{\boldsymbol{\varepsilon}})d\Omega = 0 \tag{3}$$

If $\boldsymbol{\varepsilon}$ is a continuous function, then an approximation function (shape function) $\mathbf{N}$ can be introduced to relate the value of $\boldsymbol{\varepsilon}$ at any location to its nodal values $\boldsymbol{\Sigma}$:

$$\boldsymbol{\varepsilon} = \mathbf{N}.\boldsymbol{\Sigma} \tag{4}$$

By substituting equation (4) into equation (3), the integral equation can be written in a matrix form as:

$$\mathbf{K}\boldsymbol{\Sigma} = \mathbf{R} \tag{5}$$

where

$$\mathbf{K} = \int_{\Omega} \mathbf{N^P}\mathbf{v}.\nabla\mathbf{N}d\Omega$$

$$\mathbf{R} = \int_{\Omega} \mathbf{N}^{\mathbf{P}} \dot{\varepsilon} d\Omega$$

In conventional FE discretization, the Galerkin formulation is widely used where $\mathbf{N}^{\mathbf{P}}$ is taken to be equal to the shape function **N**. However, this may result in non-physical oscillations in the solution if the partial differential equation contains a convection term. The streamline upwind Petrov–Galerkin (SUPG) scheme is used here to stabilize the solution [16]. In the SUPG scheme, the weighting function comprises the interpolation terms plus an additional mesh-dependent term:

$$\mathbf{N}^{\mathbf{P}} = \mathbf{N}^{T} + \tau \mathbf{v}.\nabla \mathbf{N}^{T} \tag{6}$$

The weighting function in this scheme is designed to include the upwinding effect. It is based on the idea of allowing more weight to nodes in the upstream direction and reducing the weight for nodes in the downstream direction. The upwinding scheme is motivated by examination of the classical advection-diffusion equation. The solution of this equation is oscillatory in space when a mesh parameter known as the Peclet number exceeds a critical value.

The Peclet number P_e can be defined as follows:

$$P_e = \frac{h_e}{\alpha \left\| \mathbf{v} \right\|_2} \tag{7}$$

where α is the diffusivity, h_e is the characteristic length of an element and $\left\| \bullet \right\|_p$ is the P-norm (for p = 2 we get the Euclidean norm and when $p \to \infty$ we get the maximum norm). The reader should be aware that there are different definitions for the characteristic element length h_e for a 2D element in the literature and here we have taken h_e as the characteristic distance in the direction of the flow. This is based on the argument that the oscillations in the numerical solution are generated by the high Peclet number in the streamline direction [13]. For a triangular element with a natural local coordinates system (see Appendix I), it can be demonstrated that h_e is given by:

$$h_e = \frac{\|\mathbf{v}\|_2}{\|\nabla\zeta.\mathbf{v}\|_\infty} \tag{8}$$

where ζ represents the local coordinates and $\nabla\zeta$ is the element mapping matrix.

Based on this definition for the element characteristic length, the parameter τ in equation (6) can be defined as a function of the element size and the velocity as follows:

$$\tau = \beta \frac{h_e}{2\|\mathbf{v}\|_2} \tag{9}$$

where β is strictly non-negative and can be related to the element Peclet number P_e as:

$$\beta = \chi\left(\coth\left(\frac{P_e}{2}\right) - \frac{2}{P_e}\right) \tag{10}$$

where χ is a smoothing parameter controlling the artificial diffusion.

Substituting equation (10) into (9) gives:

$$\tau = \frac{\beta}{2\|\nabla\zeta.\mathbf{v}\|_\infty} \tag{11}$$

It should be noted that with $\chi = 1.0$, equations 6-10 give exact nodal solutions in one-dimensional analysis (see [11] for example). Existence of an exact solution cannot be proven in multi-dimensions. However, as will be demonstrated later $\chi = 1.0$ provides sufficient accuracy in 2D analysis unless there is a significant strain tensor gradient normal to the direction of the flow. In such cases, judicious choice of χ might be required. An alternative approach to tackle significant changes in the field variable normal to the direction of the flow is proposed by Hughes et al. [16] who modified the SUPG scheme by adding an extra term called the "discontinuity-capturing operator" to the weighting function. Hughes et al. [16]

called their modified scheme Beyond Streamline Upwind Petrov Galerkin (BSUPG). The BSUPG scheme requires the gradient of the field variable to be calculated iteratively hence this makes the scheme extremely expensive in terms of CPU time. Even so, there is no guarantee that an accurate solution may be achieved, as demonstrated by Hendriana [20]. As will be demonstrated later, however, an appropriate choice of χ gives a reasonably accurate solution without the need to conduct expensive iterative calculations.

Comparison with analytical solutions

The new SUPG formulation for evaluating strain is compared with existing analytical solutions for a number of penetrometer problems. The SUPG formulation is implemented in Wolfram MATHEMATICA V9.0. In the SUPG analysis, the results are obtained assuming insignificant diffusivity $\alpha = 10^{-10}$ (equation 7). Unless stated otherwise, the smoothing parameter χ is taken to be equal to 1.0.

Simple Pile Problem

To develop a better understanding of the mechanisms of deep penetration, Baligh [2] derived the solid simple pile solution (Figure 1) to investigate deep steady quasi-static undrained penetration of an axisymmetric cylindrical object with a rounded tip in saturated (incompressible) homogeneous isotropic clay initially subjected to an isotropic state of stress.

The streamline locations are given by:

$$r^2 = r_0^2 + \frac{1}{2} R^2 (1 + \cos\phi) \tag{12}$$

where $\phi = \tan^{-1}\left(\frac{r}{z}\right)$

and the radius of the pile r_p is given by:

$$r_p^2 = \frac{1}{2} R^2 (1 + \cos\phi) \tag{13}$$

where R is a constant and the pile tip is located at a depth $z = -R/2$

The velocity components are given by:

$$V_r = \frac{V_0 R^2}{4\rho^2} \sin\phi \tag{14}$$

$$V_z = \frac{V_0 R^2}{4\rho^2} \cos\phi + V_0 \tag{15}$$

The strain can be found from the integration of the strain rates:

$$\varepsilon_{ij} = \int_0^t \dot{\varepsilon}_{ij} dt \tag{16}$$

which can be transformed to spatial integration (See [5]):

$$\varepsilon_{ij} = \int_S \frac{\dot{\varepsilon}_{ij}}{V} dS = \int_\phi^\pi \dot{\varepsilon}_{ij} \frac{\rho}{V_r \cos\phi - V_z \sin\phi} d\phi \tag{17}$$

Therefore, the strain components are given by:

$$\varepsilon_r = \int_\phi^\pi (3\cos 2\phi - 1) A(\phi) d\phi$$

$$\varepsilon_z = \int_\phi^\pi -(1 + 3\cos 2\phi) A(\phi) d\phi$$

$$\varepsilon_\theta = \int_\phi^\pi 2A(\phi) d\phi$$

$$\varepsilon_{rz} = \int_{\phi}^{\pi} -3A(\phi)\sin 2\phi d\phi \tag{18}$$

where

$$A(\phi) = \frac{\mathrm{R}^2 \sin\phi}{4(\mathrm{R}^2 + 2\mathrm{r}_0^2 + \mathrm{R}^2\cos\phi)}$$

Figure 2 shows the finite element mesh used in the calculations. The mesh comprises 2000 6-noded triangular elements. The integration over each element was carried out using 12 Gaussian points. Since the basic differential equation (equation 1) is a first order equation, only one boundary condition is required. Material entering the region is assumed to be undeformed: $\boldsymbol{\varepsilon} = \mathbf{0}$. A large domain is selected in the SUPG calculations since the analytical solution is derived assuming an unbounded domain.

Figures 3 and 4 show the SUPG predictions for strain components compared with the analytical solution (equation 18) along two streamlines $r_0/R \approx 2$ and $r_0/R \approx 10.4$. In both cases, the SUPG predicts are in excellent agreement with the analytical solution.

T-bar problem

There is increasing popularity in using full-flow penetrometers such as the cylindrical T-bar [21]. One of the reason is that the resistance of the T-bar is not influenced significantly by the soil rigidity ratio ($I_r = G/s_u$, where G and s_u are the shear modulus and undrained strength of the soil) unlike classical cone penetrometers and the shaft has little effect on the measured resistance.

Klar and Osman [8] derived a continuous velocity field for steady-state conditions using Airy stress functions. For smooth contact between the T-bar and the surrounding soil, the velocity components are given by

$$V_r = \frac{U_{Tbar}}{A}\frac{(R^2-r^2)(r^2R^2+r_0^4)+2r^2(R^4+r_0^4)\ln\frac{r}{R}}{r^2}\cos\theta$$
$$V_\theta = \frac{U_{Tbar}}{A}\frac{(r^2-R^2)(3r^2R^2-r_0^4)-2r^2(R^4+r_0^4)\ln\frac{r}{R}}{r^2}\sin\theta \qquad r_0 \le r \le R \qquad (19)$$

where

$$A = R^4 - r_0^4 + 2(R^4+r_0^4)\ln\frac{r_0}{R}$$

with r_0 the radius of the T-bar and R the distance to the zero displacement boundary of the velocity field. For a smooth interface between the penetrometer and the surrounding soil, R is found to be equal to $2.4r_0$.

For the case of full-bonding contact:

$$V_r = \frac{U_{Tbar}}{B}\frac{(R^2-r^2)(r^2+r_0^2)-2r^2(R^2+r_0^2)\ln\frac{r}{R}}{r^2}\cos\theta$$
$$V_\theta = \frac{U_{Tbar}}{B}\frac{(r^2-R^2)(3r^2-r_0^2)-2r^2(R^2+r_0^2)\ln\frac{r}{R}}{r^2}\sin\theta \qquad (20)$$
$$B = R^2 - r_0^2 + (R^2+r_0^2)\ln\frac{r_0}{R}$$

At the limiting state, R is found to be equal to $2.85r_0$.

Figure 5 shows the mesh used in the SUPG analysis. The mesh comprises 800 6-node elements with 1681 nodes in total. The outer radius R was taken to be equal to $2.4r_0$ in the case of a smooth T-bar and $2.85r_0$ for a perfectly rough T-bar. The boundary condition is defined as:

$$\boldsymbol{\varepsilon} = \mathbf{0} \quad at\left(0 \le \theta \le \frac{\pi}{2} \quad \& \quad r = R\right) \qquad (21)$$

Figure 6 shows the contours of the cumulative absolute (plastic) shear strain, ξ, which is defined as:

$$\xi = \int_t |\dot{\gamma}_{\max}| dt = \int_t \sqrt{(\dot{\varepsilon}_x - \dot{\varepsilon}_y)^2 + 4\dot{\varepsilon}_{xy}}\, dt$$
$$\dot{\varepsilon}_x = \frac{\partial V_x}{\partial x}; \dot{\varepsilon}_y = \frac{\partial V_y}{\partial y}; \dot{\varepsilon}_{xy} = \frac{1}{2}\left(\frac{\partial V_x}{\partial y} + \frac{\partial V_y}{\partial x}\right) \quad (22)$$

Figure 6a shows the analytical solution obtained by integrating along the streamline of the velocity field of Klar and Osman [8]. The analytical solution shows that the extreme case of full bonding contact between a moving T-bar and the surrounding soil is characterised by a high shear strain gradient normal to the direction of flow in the wake-zone behind the penetrometer, while there is a more gradual gradient in the case of a smooth contact. Figure 6b shows the numerical solution obtained without the need to adjust the smoothing parameter (i.e. $\chi = 1.0$) for the case of smooth contact. However, for the full-bonding case, the solution is obtained by using $\chi = 3.0$ in order to get smooth contours. Figure 6b shows that the SUPG formulation is capable of capturing the details of the shear strain contours. Figure 7 shows contours of accumulative shear strain obtained using different smoothing parameters ranging from $\chi = 1.0$ to $\chi = 10.0$. As may be seen from this figure, only a very small region behind the T-bar needs smoothing. Apart from this region, the solution is not affected by the choice of χ.

The new SUPG formulation can be used as a separate tool for calculating strains once the velocity field is obtained (from the strain path method, for example) or it can be integrated into finite element analysis where the velocity field is obtained by solving the momentum equation, as described below.

Analysis of Cone penetration Test in a strain-softening material

The cone penetration test is one of the most widely in-situ tests in geotechnical engineering practice for assessing the strength profile in soil. In saturated clay, the test is performed at a penetration rate that does not permit drainage during the penetration process, so the test may

be interpreted directly as a measure of the undrained strength profile of the clay. The popularity of this in situ testing device has resulted in a great demand for the development of accurate correlations between measured cone quantities (e.g., cone resistance and sleeve friction ratio) and engineering properties of the soil. Despite extensive research on cone penetration test in the last two decades [6, 22-27] the effect of strain softening on the cone resistance has not been investigate in detail.

In strain-softening material, the strength of the soil can be expressed as a function of the cumulative plastic strain. Einav and Randolph [7] suggested a simple function of the form:

$$s_u = s_{u0}\left(\delta_{rem} + (1-\delta_{rem})e^{-3\xi/\xi_{95}}\right) \tag{23}$$

where the ratio ξ/ξ_{95} is the ratio of the measure of current accumulative plastic strain normalised by a reference value. Einav and Randolph [7] took the cumulative engineering shear strain ξ (defined in equation (22)) as the measures of cumulative strain for a Tresca material, compared with the von Mises model adopted here. ξ_{95} is the cumulative shear strain required to cause 95% reduction (from peak value to remoulded). δ_{rem} represents the fully remoulded strength ratio (i.e. $s_{u(remolded)}/s_{ui}$) or the inverse of the sensitivity index, S_t,

In this paper we will evaluate the effect of strain softening on the cone resistance using two approaches:

(1) an approximate approach analogous to the upper bound strain path method (UBSPM) of Einav and Randolph [7] and Klar and Osman [8]. Since there is no existing closed form solution for the velocity field around the cone, the velocity field and the strain rate were obtained from Eulerian finite element analysis assuming a perfectly plastic material.

(2) By implementing directly a strain-softening constitutive model into a large-strain finite element analysis.

The first approach is approximate but it allows exploring different strain-softening constitutive relationships from a single velocity field obtained from FE analysis.

FE model

Figure 8 shows the finite element mesh used in the analysis. The mesh consisted of 1701 nodes and 800 six noded reduced integration triangular elements. The outer boundary was fixed in the radial direction. Displacement controlled analysis was performed and the cone is taken be stationary. A standard 60^o cone with a smooth interface between cone and soil was simulated. Soil movement normal to the cone-soil interface was prevented and only sliding motion allowed. The radial distance to the outer boundary was chosen to be well outside the plastic zone. Based on cavity expansion analysis [28] the ratio of plastic radius to the current cavity radius remains constant at $\sqrt{I_r}$. The radial distance was taken to be 30R which is wide enough for the range of rigidity index between 50 and 500, which was investigated in the finite element simulations. Isotropic initial stress states were assumed.

In all the analysis a linear elastic model with von Mises failure criterion was assumed:

$$f = q - \sigma_y = 0 \tag{24}$$

where q is the deviatoric shear strain defined as:

$$q = \sqrt{\frac{2}{3} s_{ij} : s_{ij}} \tag{25}$$

with s_{ij} the deviator stress ($s_{ij} = \sigma_{ij} - \sigma_{kk}\, \delta_{ij}/3$). The von Mises yield stress (σ_y) is equivalent to twice the undrained shear strength of the soil s_u in triaxial compression test (i.e. $\sigma_y = 2s_u$).

Figure 9 shows the load displacement curve obtained from the enhanced Eulerian FE analysis compared with that obtained from small strain Lagrangian analysis using the same boundary conditions. The results are shown for $I_r = 100$. In the large-strain Eulerian FE analysis, the thin-plate spline technique [29, 30] was used to calculate the gradient of the stress. The accuracy of the small-strain analysis becomes doubtful for displacements beyond 0.5D, because of the gross distortion of the mesh, as indicated by the divergence of the two curves. With the small strain assumption it is not possible to reach the limiting resistance of the cone tip. In large-strain analysis, the limiting resistance is not achieved until a penetration of

approximately 7D, beyond which the normalised penetration resistance is reasonably constant at about 10.5.

It is well established that the rigidity index of the soil has a significant influence on the cone factor. This effect has been quantified by carrying out a series of analyses for different values of rigidity indices as shown in Figure 10. The Eulerian FE results are compared with published correlation formulae as detailed in Table 1 (for conditions of a smooth cone-soil interface and originally isotropic stress state). These results illustrate that the current Eulerian analysis, enhanced with the thin-plate spline technique, gave results that are consistent with the 'remeshing and interpolation technique combined with small strain' (RITSS) analysis of Lu et al. [25] and the Arbitrary Lagrangian Eulerian ALE analysis of Nazem et al. [27].

Figure 11a shows the streamlines around the cone. It should be noted that in this analysis the cone is treated as stationary while the soil flows around it. Figure 11b shows the magnitude of the velocity under steady-state conditions normalised by the inlet velocity. As can be seen from this figure, the change of velocity field is localised around the cone tip. Figure 12 shows contours of the rate of the plastic deviatoric strain (normalised by v_0/D).

An approximate approach for evaluating the effect of the strain softening

As demonstrated earlier in the paper, the SUPG approach allows calculation of the cumulative strain once the strain rate is known. The cumulative strain can be evaluated from the strain rate shown in Figure 12 by applying equation (5):

$$\left(\int_{\Omega} \mathbf{N}^{\mathbf{P}} \mathbf{v}.\nabla \mathbf{N} d\Omega\right) \boldsymbol{\Sigma}_q^p = \left(\int_{\Omega} \mathbf{N}^{\mathbf{P}} \dot{\varepsilon}_q^p d\Omega\right) \tag{26}$$

where $\boldsymbol{\Sigma}_q^p$ is the accumulative plastic deviatoric strain at the element nodal points.

Figure 13 shows contours of cumulative plastic strain at steady state conditions for $I_r = 100$ and $I_r = 300$. If the degradation of the undrained shear strength is taken to be governed by

equation (23) and the internal variable ξ is taken equivalent to the plastic deviatoric strain (i.e. $\xi = \varepsilon_q^p$), then the strength distribution in space can be mapped using the contours of accumulated strain shown in Figure 13. The penetration resistance can then be estimated, as in the conventional upper bound approach, by integrating the internal work within the domain, and balancing external work and total internal plastic work:

$$\int_{\Omega} \sigma_y(\varepsilon_q^p)\dot{\varepsilon}_q^p d\Omega = F_t v_0 \tag{27}$$

where F_t is the tip resistance and v_0 is the inlet velocity.

Figures 14 shows the effect of strain-softening expressed as the cone resistance normalised by its value when there is no softening and plotted against different reference plastic strain ξ_{95} for remoulding ratios δ_{rem} of 0.2 and 0.5. Figure 14a shows the results for I_r = 100 while the results for I_r = 300 are shown in Figure 14b. Comparing 14a and 14b indicates that the rigidity index has little influence on the pattern and the magnitude of the degradation of cone resistance due to strain softening. A typical range of reference plastic strain ξ_{95} in clay is between 10 and 50 (see [7]). The results of Figure 14 indicate that even with a soil of high sensitivity ratio δ_{rem} = 0.2, the maximum reduction in the cone resistance due to strain softening is less than 10%. This is significantly less than for a full-flow penetrometer [31].

It should be noted that the velocity field used to derive the limiting resistance in strain-softening materials is not optimised for the lowest upper bound solution (i.e. lowest limiting cone resistance). Furthermore, the area of plastic zone is approximated. In this calculation, 6 node triangular elements with reduced integration points are used. Thus, if a single Gaussian point in a certain element becomes plastic, it is then assumed that the plastic region represents one third of that element.

Nevertheless, the upper bound calculations may be used as a first estimate of softening effects. More accurate evaluation of the strain-softening effect can be obtained by implementing a strain-softening model in the FE analysis.

Eulerian FE analysis of a cone in a strain softening material

Von Mises material with strain softening given by equation (23) can be implemented in the FE analysis. However, the internal variable ξ needs to be tracked and updated in each time increment during the analysis. The material derivative of ξ can be written as:

$$\dot{\xi} = \frac{\partial \xi}{\partial t} + v_k \xi_{,k} = \Lambda \tag{28}$$

where Λ is evaluated from the constitutive relations and the consistency condition.

The operator splitting technique [32] can be used to solve the above equation. Equation (28) can be decomposed into sets of simple partial differential equation operators, which can be solved sequentially as follows:

$$\begin{aligned} \dot{\xi} &= \Lambda \\ \frac{\partial \xi}{\partial t} + v_k \xi_{,k} &= 0 \end{aligned} \tag{29}$$

The first set can be solved without considering the convective effect thus it can be evaluated in the same manner as in an updated Lagrangian analysis.

The consistency condition requires that:

$$\dot{f} = \frac{\partial f}{\partial \boldsymbol{\sigma}} : \dot{\boldsymbol{\sigma}} + \frac{\partial f}{\partial \xi} : \dot{\xi} = 0 \tag{30}$$

where *f* is the yield function and the stress increment is given by:

$$\dot{\boldsymbol{\sigma}} = D^e : \dot{\varepsilon} - D^e : \dot{\lambda} \frac{\partial g}{\partial \boldsymbol{\sigma}} \tag{31}$$

where D^e is the elastic stiffness matrix, g is the plastic potential and $\dot{\lambda}$ is the Lagrangian plastic multiplier. In a von Mises material $\dot{\lambda}$ can be taken to be equal to the plastic deviatoric strain rate (i.e. $\dot{\lambda} = \dot{\xi} = \dot{\varepsilon}_q^p$)

For a von Mises material with associated flow rule and strength softening according to equation (23), equations (29) and (30) can be re-written as:

$$q^{tr} - \sigma_y - 3G\Delta t\dot{\xi} + \sigma_{y0}\frac{3\Delta t\dot{\xi}}{\xi_{95}}(1-\delta_{rem})e^{-3\xi/\xi_{95}} = 0 \tag{31}$$

where q^{tr} is the trial elastic deviatoric stress lying outside the yield surface (i.e. plastically inadmissible stress) and

$$\dot{\lambda}\Delta t = \frac{q^{tr} - \sigma_y(\xi + \dot{\xi}\Delta t)}{3G - \dfrac{3\sigma_{y0}}{\xi_{95}}(1-\delta_{rem})e^{-3\xi/\xi_{95}}} \approx \frac{q^{tr} - \sigma_y(\xi)}{3G} \tag{32}$$

We can derive the above approximation by noting that $\Delta t\dot{\xi} << \xi_{95}$ for small displacement increment (i.e. $\Delta t v_0 << D$). Therefore, ξ is updated by:

$$\xi(t+\Delta t) = \xi(t) + \dot{\xi}\Delta t - v_k\Delta t\xi_{,k} \tag{33}$$

Figure 15 shows the results of the Eulerian Finite element analysis with strain softening yield criteria. The FE results are in good agreement with the upper bound solution. This demonstrates the consistency of the strain-softening formulation given by equations (28-33).

Comparison with T-bar

The upper bound based strain path method of Einav and Randolph [7] and the large-strain finite element analysis of Zhou and Randolph [31] show that the reduction in the limiting resistance of a T-bar embedded in a rate-independent material can be expressed as:

$$\frac{N_c}{N_{c0}} = \delta_{rem} + (1-\delta_{rem})e^{-1.5\xi_T/\xi_{95}} \quad (34)$$

where N_{c0} is the bearing capacity factor calculated for an ideal rigid plastic material. The parameter ξ_T reflects the average magnitude of shear strain undergone by soil elements passing through the velocity field around the T-bar. Zhou and Randolph [31] evaluated this parameter as 3.85.

Figure 16 shows the effect of strain softening for the T-bar. The FE results were obtained using the mesh shown in Figure 5 with an outer radius R = $60r_0$. The stress integration was carried out using three Gaussian points per element. The FE results are reasonably consistent with Zhou and Randolph [31]. However, it should be borne in mind that the FE results were obtained here using the von Mises failure criterion and the softening parameter ξ is taken to be equivalent to the plastic deviatoric strain, while in Zhou and Randolph [31] the Tresca model was used and ξ was taken as the plastic engineering shear strain.

Figure 17 compares the effect of strain softening in the cone penetration test and in the T-bar as given by equation 34. The figure shows that the effect of softening in the CPT is much lower than for the T-bar. The reduction in cone-resistance is about 20 % of the reduction in T-bar resistance for the case of δ_{rem} = 0.5.

Conclusions

A methodology for evaluating strains around steady-state penetrometers has been proposed. The key advantage of the proposed formulation is that the strain components can be calculated directly from the strain rate defined in terms of small strain theory. Rather than building streamlines for back integration, as in the conventional strain path method, the new technique treats the domain as continuous with the associated field equations. There is no need to carry out the calculations in any topological order. All that is needed is to assemble the two matrices K and R given by equation (5). Another advantage of the proposed technique is that it can be integrated into the finite element calculations.

The effect of strain-softening in the cone penetration test has been evaluated using two methods: (i) An approximate approach analogous to a classical upper bound solution, but with the velocity field obtained from a large-strain finite element formulation assuming a

perfectly plastic model. The reduction of soil strength is then estimated by mapping the contours of cumulative plastic strain. (ii) A large-strain formulation with strain-softening constitutive model. Both approaches give consistent results and show that the effect of softening is much less significant for the cone penetration test compared to T-bar penetration. The reduction in cone resistance due to strain-softening is about 20 % of the reduction in T-bar resistance for the case of a sensitivity index of 2.

Acknowledgements

This work forms part of the activities of the Centre for Offshore Foundation Systems (COFS) at the University of Western Australia, currently supported as a node of the Australian Research Council Centre of Excellence for Geotechnical Science and Engineering, and by the Lloyd's Register Foundation. The study was carried out while the first author was a Martin Fahey Visiting Fellow at the Centre for Offshore Foundation Systems, the University of Western Australia.

Appendix I: Triangular elements

The triangular local coordinates are denoted by ζ_1, ζ_2 and ζ_3 which satisfies $\zeta_1+\zeta_2+\zeta_3=1$ (see Figure 18).

The element mapping matrix $\nabla\zeta$ is defined as:

$$\nabla\zeta=\begin{bmatrix}\dfrac{\partial\zeta_1}{\partial x} & \dfrac{\partial\zeta_1}{\partial y}\\ \dfrac{\partial\zeta_2}{\partial x} & \dfrac{\partial\zeta_2}{\partial y}\\ \dfrac{\partial\zeta_3}{\partial x} & \dfrac{\partial\zeta_3}{\partial y}\end{bmatrix} \tag{35}$$

which can be evaluated from the following system of linear equations:

$$\begin{bmatrix}1 & 1 & 1\\ \sum x_i\dfrac{\partial N_i}{\partial\zeta_1} & \sum x_i\dfrac{\partial N_i}{\partial\zeta_2} & \sum x_i\dfrac{\partial N_i}{\partial\zeta_3}\\ \sum y_i\dfrac{\partial N_i}{\partial\zeta_1} & \sum y_i\dfrac{\partial N_i}{\partial\zeta_2} & \sum y_i\dfrac{\partial N_i}{\partial\zeta_3}\end{bmatrix}\begin{bmatrix}\dfrac{\partial\zeta_1}{\partial x} & \dfrac{\partial\zeta_1}{\partial y}\\ \dfrac{\partial\zeta_2}{\partial x} & \dfrac{\partial\zeta_2}{\partial y}\\ \dfrac{\partial\zeta_3}{\partial x} & \dfrac{\partial\zeta_3}{\partial y}\end{bmatrix}=\begin{bmatrix}0 & 0\\ 1 & 0\\ 0 & 1\end{bmatrix} \tag{36}$$

where **N** is the shape function and $\sum N_i = 1$.

References

1- Levadoux J. N. and Baligh, M. M., Pore pressure dissipation after cone penetration. *Dept. of Civil Engineering MIT*, 1980 Publication No R80-11.

2- Baligh, M. M., Strain path method. *Journal of Geotechnical Engineering, ASCE*, 1985; 111(9): 1108–1136.

3- Baligh, M. M., Undrained deep penetration I. shear stresses. *Geotechnique*, 1986; 36(4): 471-485.

4- Baligh, M. M., Undrained deep penetration II. pore pressure. *Geotechnique*, 1986; 36(4): 487-501.

5- Teh. C. I.; An analytical study of the cone penetration test. *PhD Thesis, Oxford University*. 1987.

6- Teh, C.I. & Houlsby, G.T; An analytical study of the cone penetration test in clay. *Geotechnique* 1991 41(1): 17-34.

7- Einav I, Randolph MF. Combining upper bound and strain path methods for evaluating penetration resistance. *International Journal for Numerical Methods in Engineering* 2005; 63(14):1991–2016.

8- Klar A, Osman AS. Continuous velocity fields for the T-bar problem. *International Journal for Numerical and Analytical Methods in Geomechanics* 2008; 32(8):949–963.

9- Klar A, Pinkert S. Steady-state solution for cylindrical penetrometers. *International Journal for Numerical and Analytical Methods in Geomechanics* 2010; 34(6):645–659.

10- Potts D. M. Numerical analysis: a virtual dream or practical reality? *Geotechnique* 2003; 53(6):535-572.

11- Belytschko T, Liu W K, Moran B, Nonlinear Finite Elements for Continua and Structures, *Wiley-Blackwell, 2000*.

12- Zhou H, Randolph MF. Resistance of full-flow penetrometers in rate-dependent and strain-softening clay. *Geotechnique* 2009; 59(2):79–86.

13- Brooks AN, Hughes TJR. Streamline upwind/Petrov–Galerkin formulation for convection dominated flows with particular emphasis on the incompressible Navier–

Stokes equation. *Computer Methods in Applied Mechanics and Engineering* 1982; 32:199–259.

14- Heinrich JC, Zienkiewicz OC. Quadratic finite element schemes for two dimensional convective-transport problems. *International Journal for Numerical Methods in Engineering* 1977; 11:1831–1844.

15- Donea J, Belytschko T, Smolinski P. A generalized Galerkin method for steady state convection–diffusion problems with application to quadratic shape functions. *Computer Methods in Applied Mechanics and Engineering* 1985; 48:25–43.

16- T.J.R. Hughes, M. Mallet and A. Mizukami, A new finite element formulation for computational fluid dynamics: II. Beyond SUPG, *Comput. Meths. Appl. Mech. Engrg.* 54 (1986) 341-355.

17- Qin X, Michaleris P. Eulerian elasto-visco-plastic formulations for residual stress prediction. *International Journal for Numerical Methods in Engineering* 2009; 63:1991-2016.

18- Agrawal A, Dawson PR. A comparison of Galerkin and streamline techniques for integration strains from an Eulerian flow field. *International Journal for Numerical Methods in Engineering* 1985; 21:853–881.

19- Bathe K J, Hendriana D, Brezzi F and Sangalli G. Inf-sup testing of upwind methods. *International Journal for Numerical Methods in Engineering* 2000; 48:745-760.

20- Hendriana D. On finite element and control volume methods for high Peclet number flows. *MSc Thesis, MIT* 1994.

21- Low, H.E. and Randolph, M.F., Strength measurement for near seabed surface soft soil, *Journal of Geotechnical and Geoenvironmental Engineering*, ASCE 2010, 136(11): 1565-1573.

22- Whittle AJ. Constitutive modelling for deep penetration problems in clay. *Proceedings of 3rd international conference on computational plasticity: fundamentals and applications*, 1992. 2:883–94.

23- van den Berg P. Analysis of soil penetration. *PhD thesis*, Delft University of Technology, Delft, The Netherlands; 1994.

24- Yu HS, Herrmann LR, Boulanger RW. Analysis of steady state cone penetration in clay. *Journal of Geotechnical and Geoenvironmental Engineering*, ASCE 2000; 126(7):594–605.

25- Lu Q, Randolph MF, Hu Y, Bugarski LC. A numerical study of cone penetration in clay. *Geotechnique* 2004; 54(4):257–67.

26- Liyanapathirana, D. S. Arbitrary Lagrangian-Eulerian based finite element analysis of cone penetration in soft clay. *Computer and Geotechnics* 2009; 36 (5): 851–860.

27- Nazem, M., Carter J. P., Airey D. W, Chow S. H. Dynamic analysis of a smooth penetrometer free-falling into uniform clay. *Geotechnique* 2012; 62(10): 893–905.

28- Vesic, A. S. Expansion of cavities in infinite soil mass. *Journal of Soil Mechanics and Foundation Division* ASCE 1972; 98(3): 265–290.

29- Duchon J, Splines minimizing rotation-invariant semi-norms in Sobolev spaces, *Lecture Notes in Mathematics* 1977, 57: 85-100.

30- Wahba G, Spline models for observational data, *CBMS-NSF Regional Conference Series in Applied Mathematics, Society for Industrial and Applied Mathematics (SIAM)*, 1990.

31- Zhou, H. and Randolph, M.F., Resistance of full-flow penetrometers in rate-dependent and strain-softening clay. *Géotechnique* 2009, 59(2): 79-86

32- Lanser D., Verwer J.G. Analysis of operator splitting for advection-diffusion-reaction problems from air pollution modelling. *Journal of Computational and Applied Mathematics* (1999); 111: 201-216.

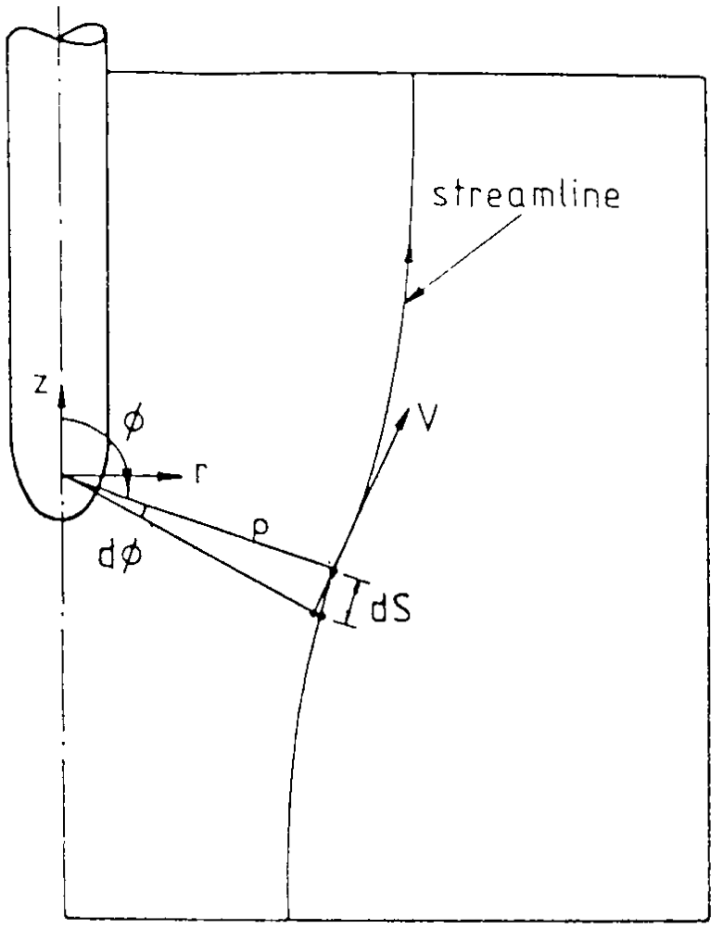

Fig 1 ‘Simple pile’ geometry [5]

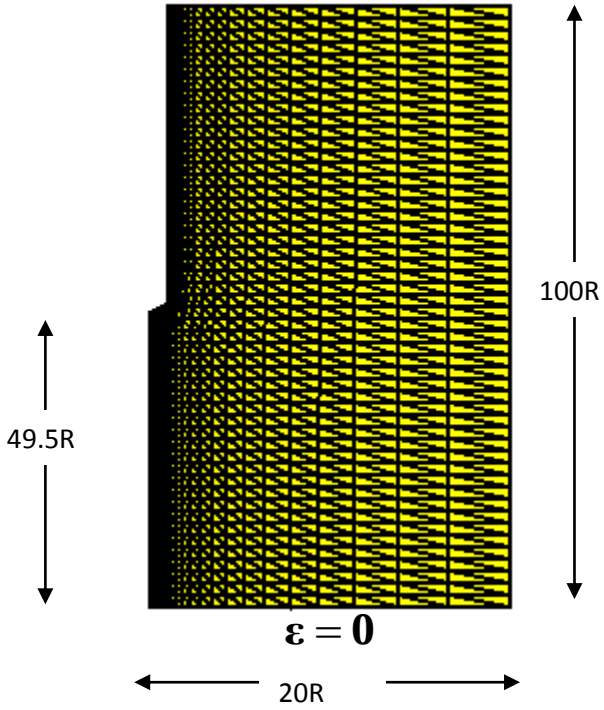

Fig. 2 Finite element mesh for simple pile problem (not to scale)

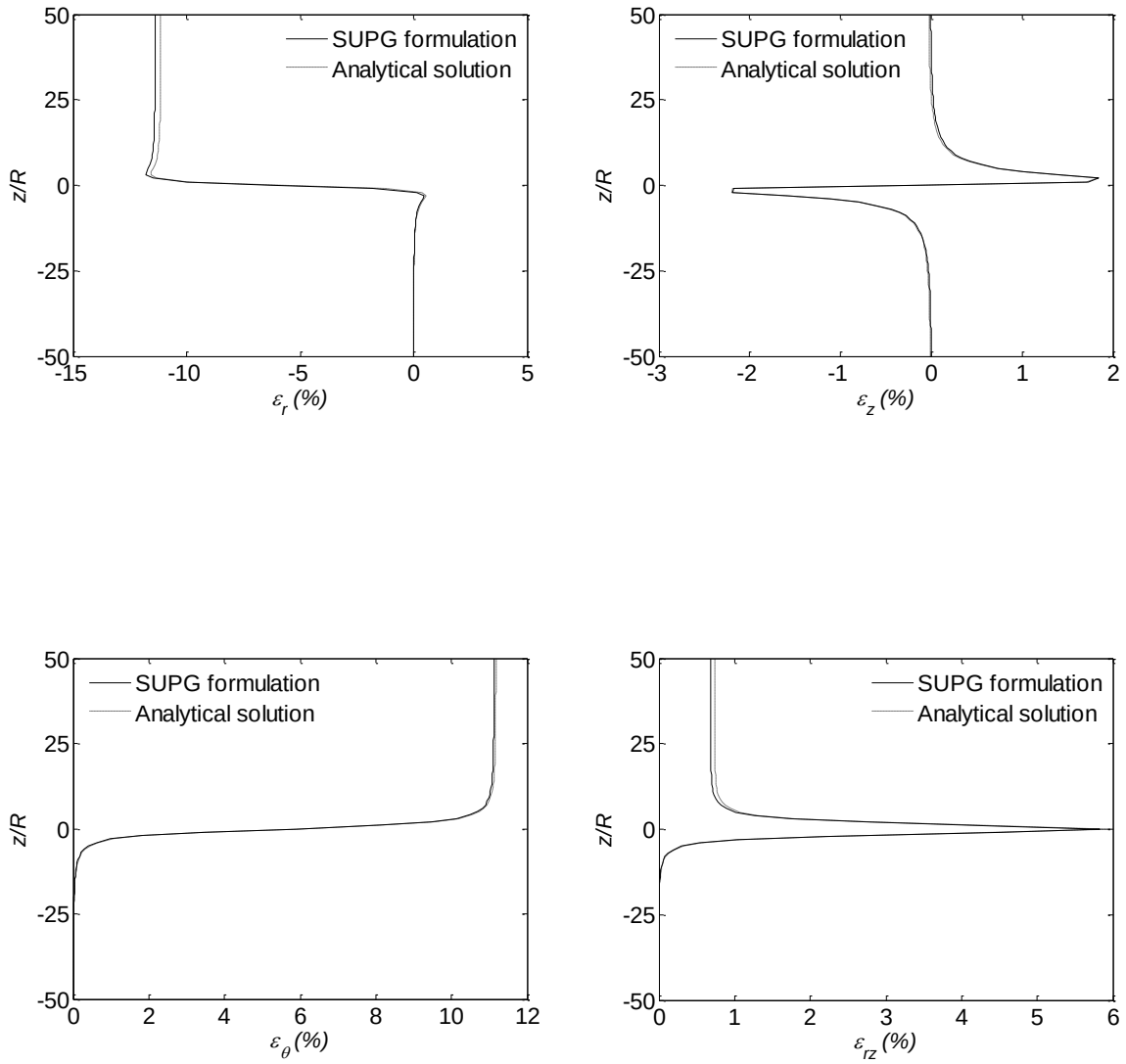

Fig. 3 Simple Pile: Comparison with analytical solution (r_0/R = 2.00)

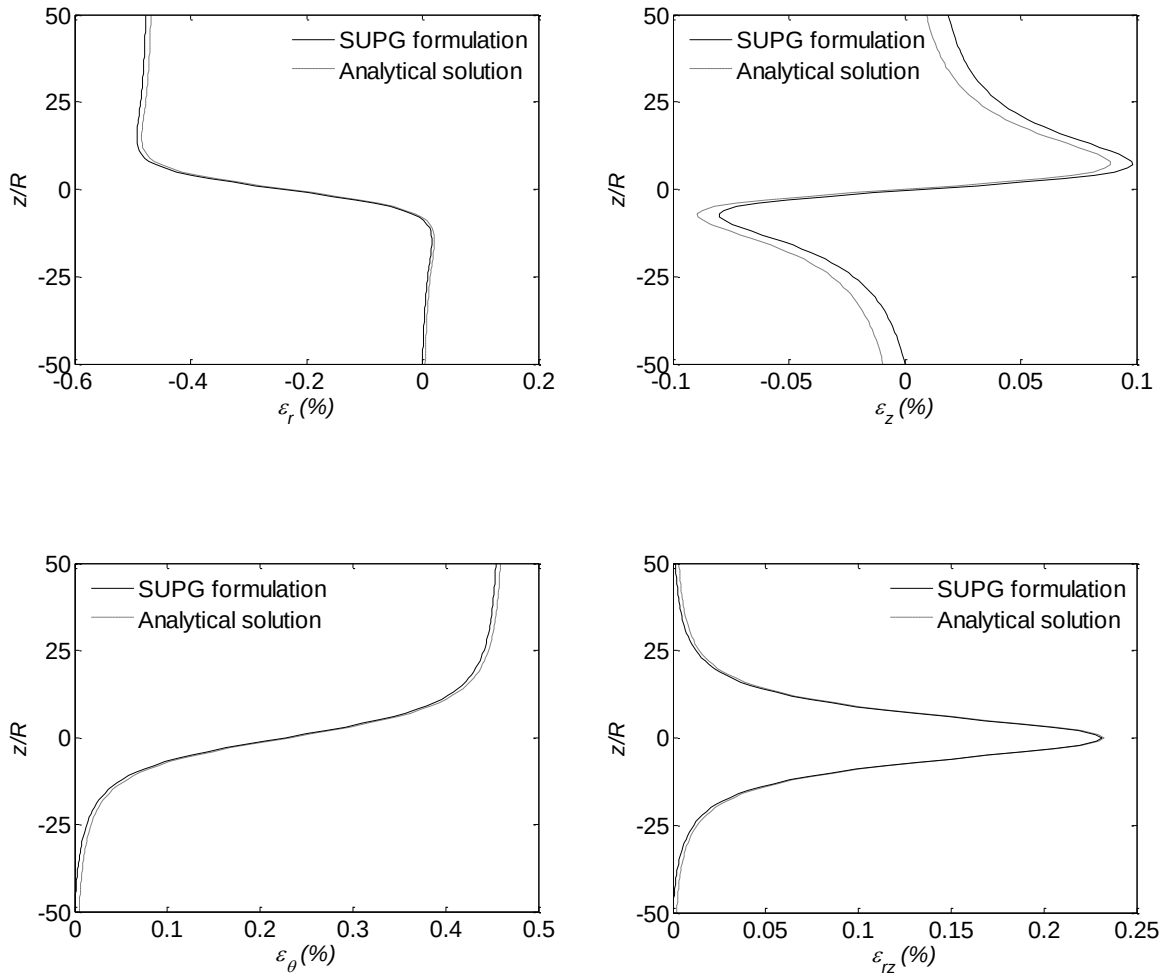

Fig. 4 Simple pile: Comparison with analytical solution (r_0/R = 10.36)

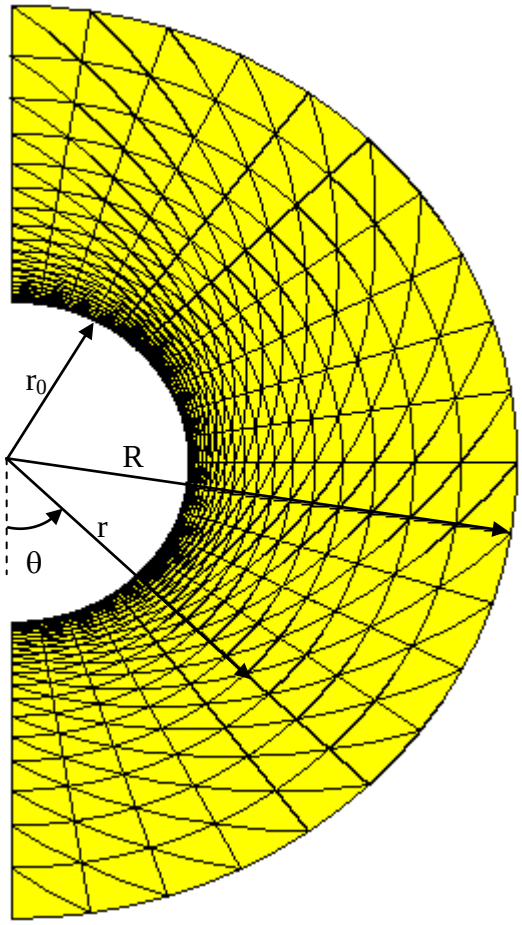

Fig. 5 Mesh used for the SUPG formulation in the T-bar problem

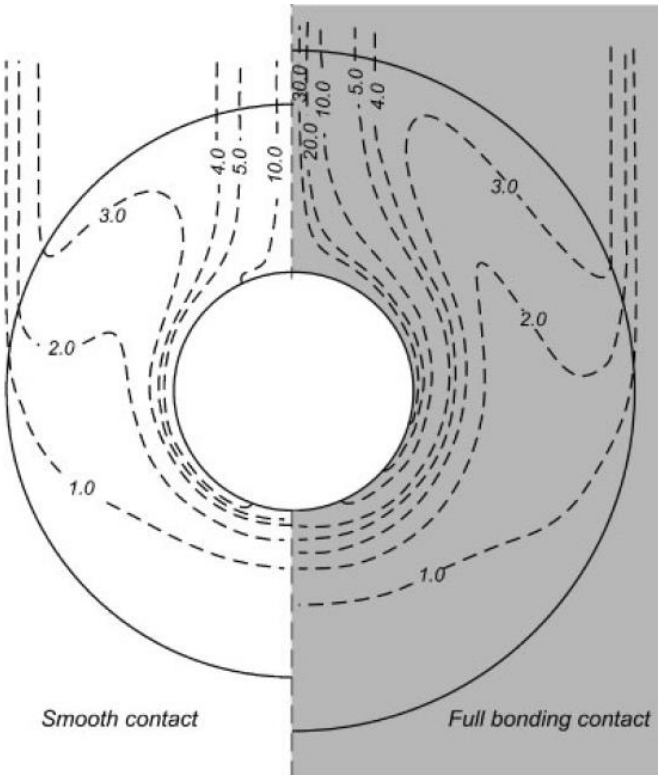

(a)

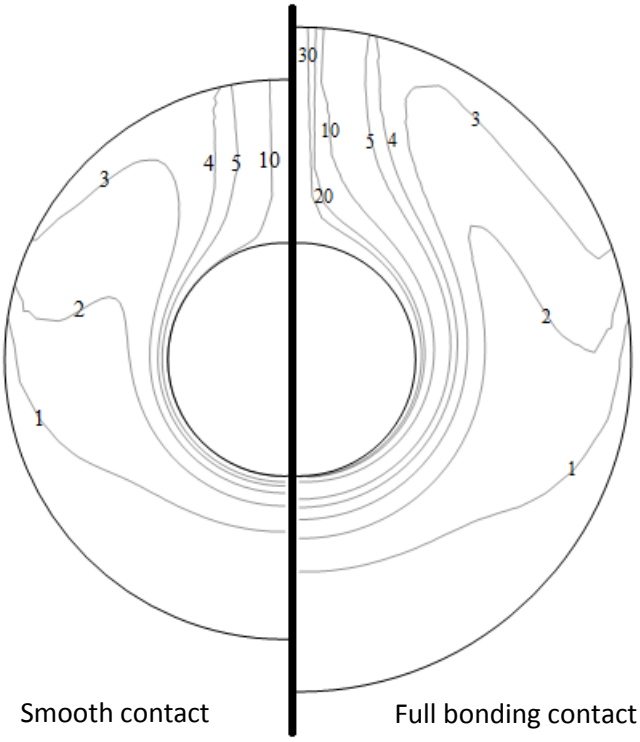

(b)

Fig. 6 Contour of accumulative shear strain (a) analytical solution (Klar and Osman 2008) (b) SUPG formulation.

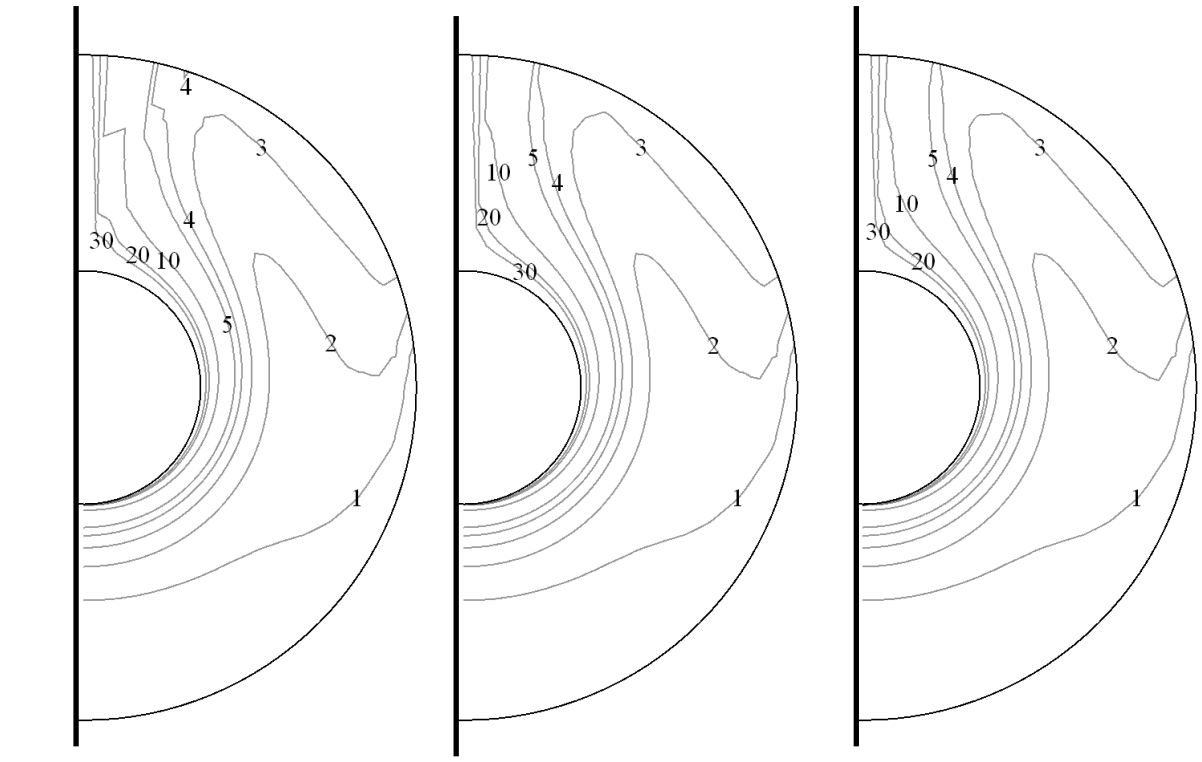

(a) χ = 1.0 (b) χ = 2.0 (c) χ = 3.0

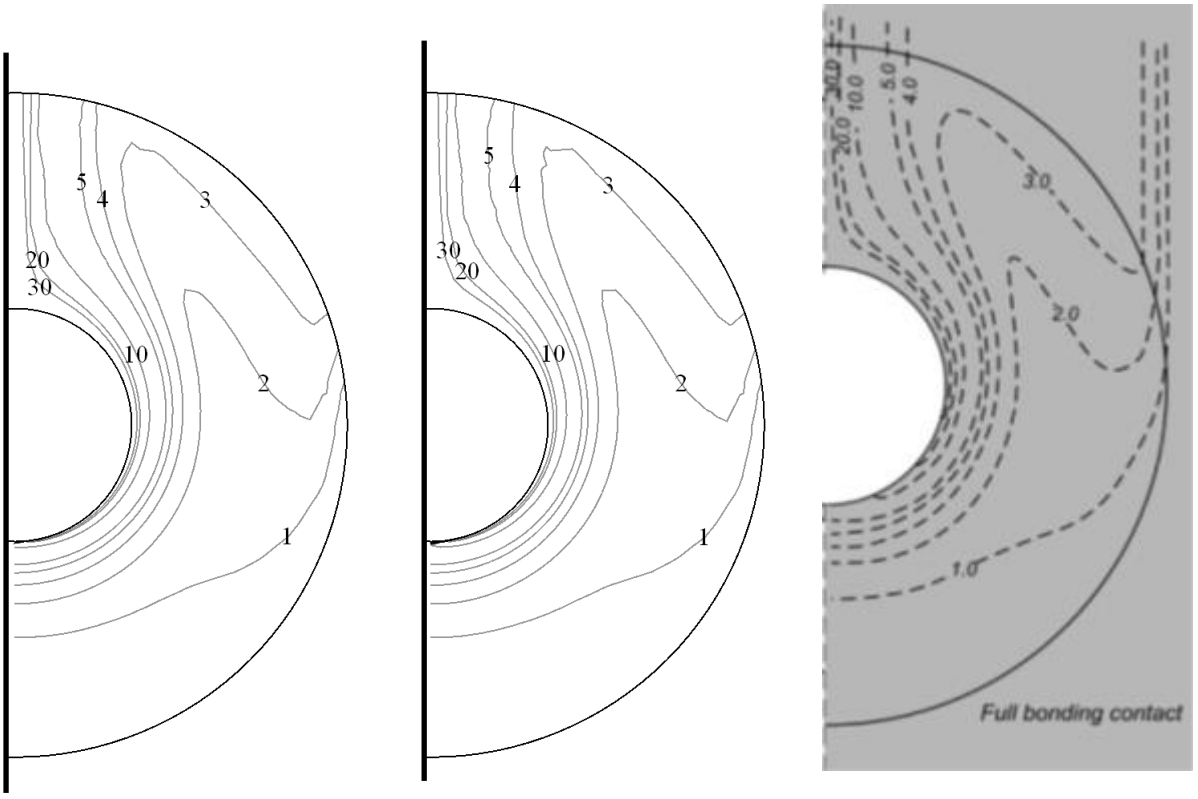

(d) χ = 5.0 (e) χ = 10.0 (f) Exact solution

Fig. 7 Effect of the smoothing parameter χ on the accumulative shear strain contours around a fully bonded T-bar.

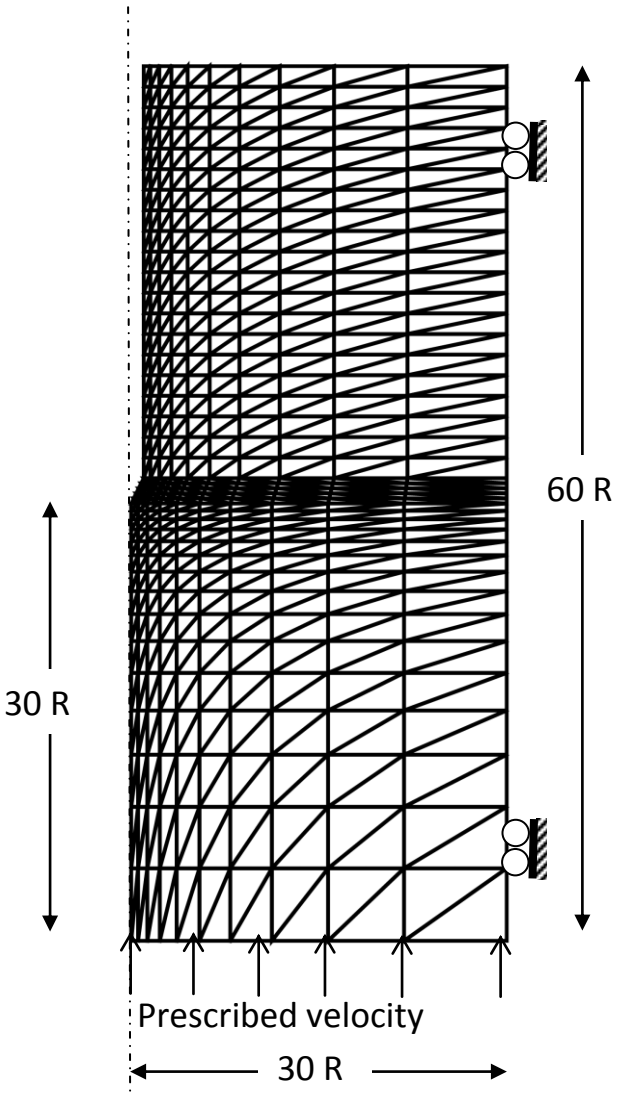

Fig. 8 Finite element mesh for CPT analysis.

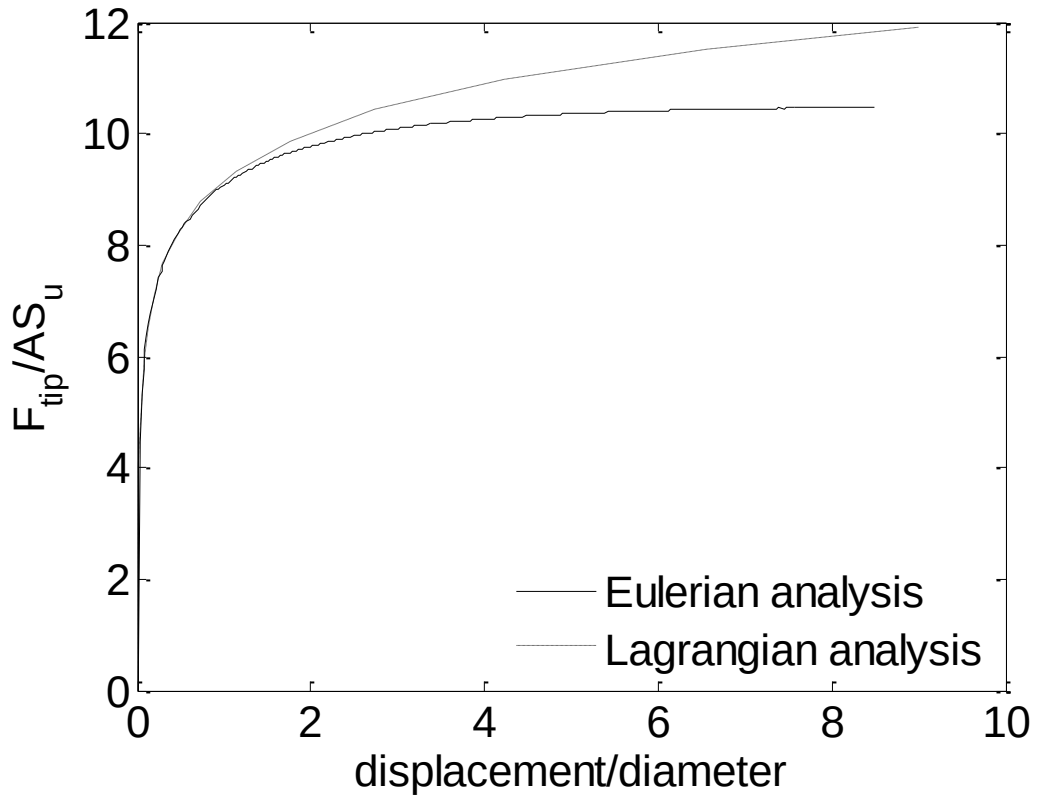

Fig. 9 Comparison between Eulerian and Lagrangian FE analysis of the CPT (I_r = 100).

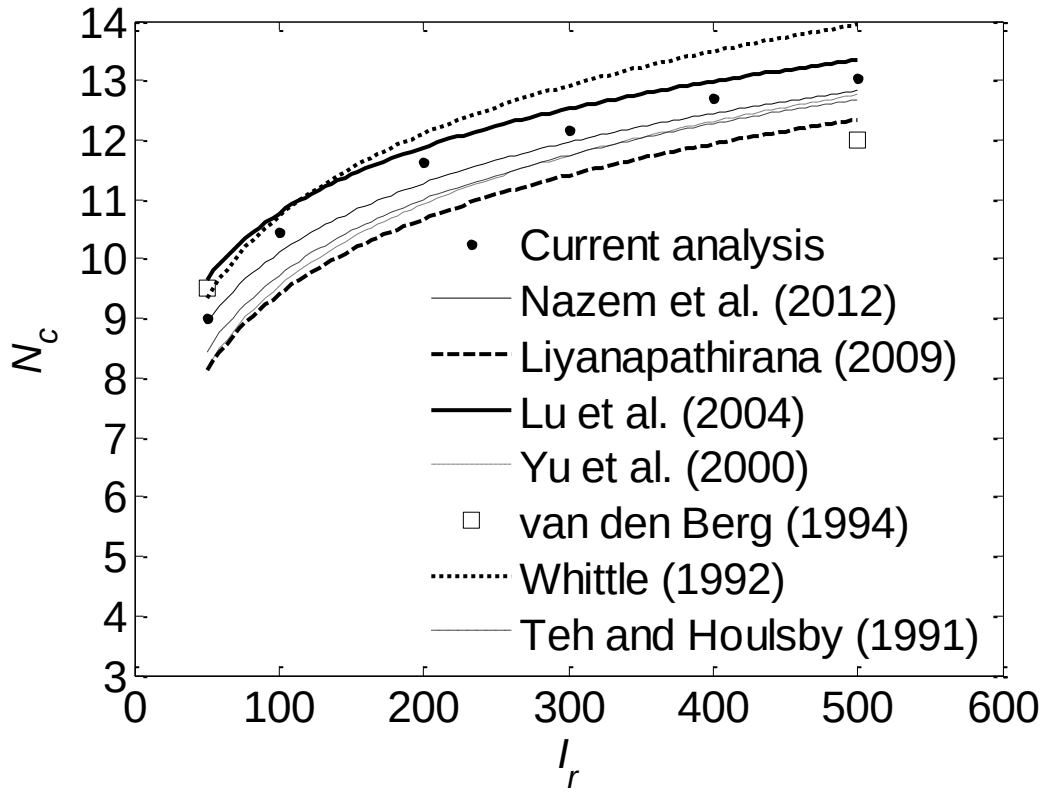

Fig. 10 Effect of rigidity index on the cone resistance.

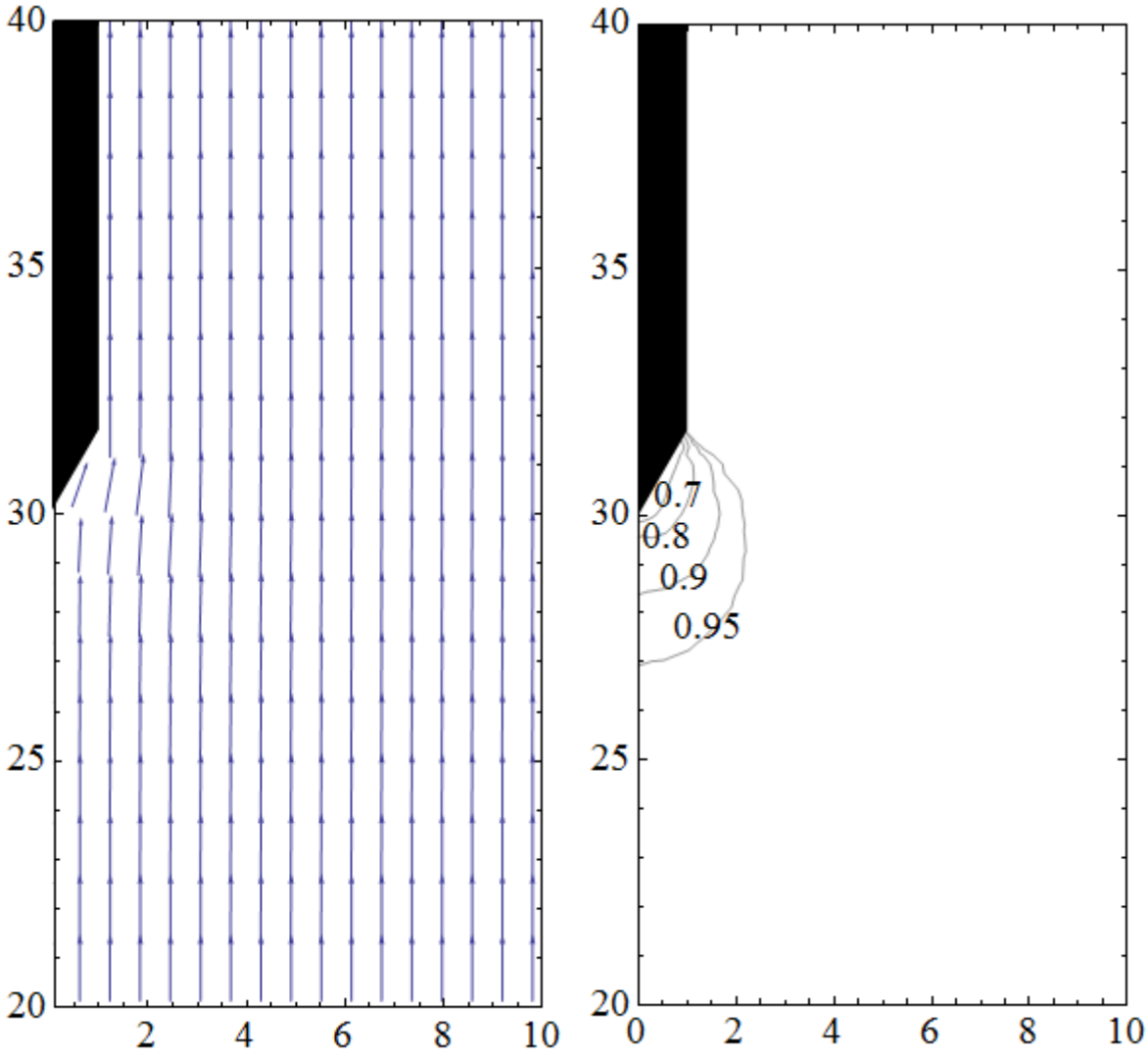

(a) (b)

Fig 11. Velocity field at steady state (I_r = 100) (a) streamlines (b) magnitude of velocity

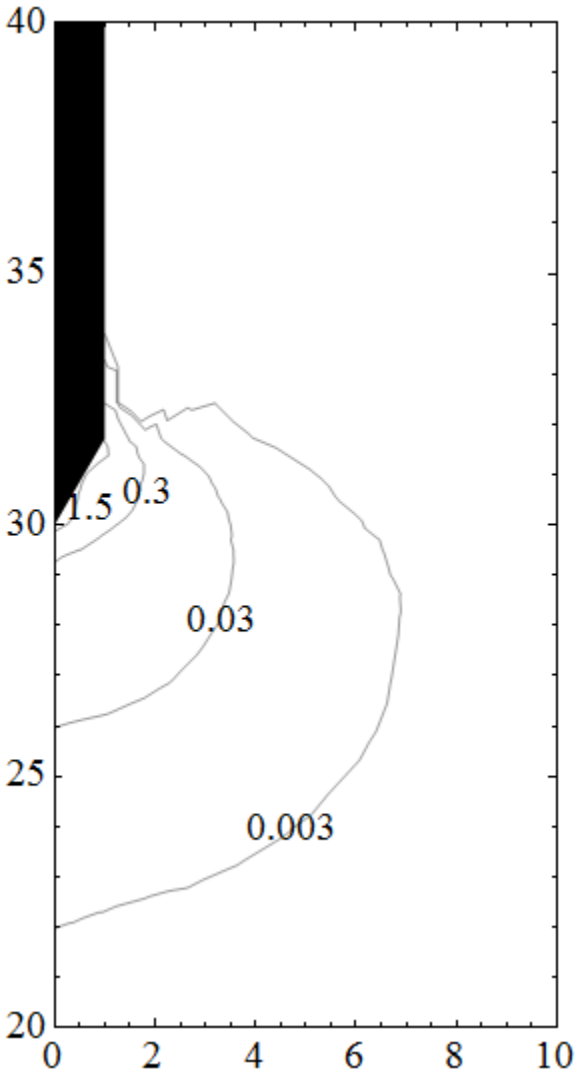

Fig 12. Contours of the rate of plastic deviatoric strain normalised by v_0/D (I_r = 100)

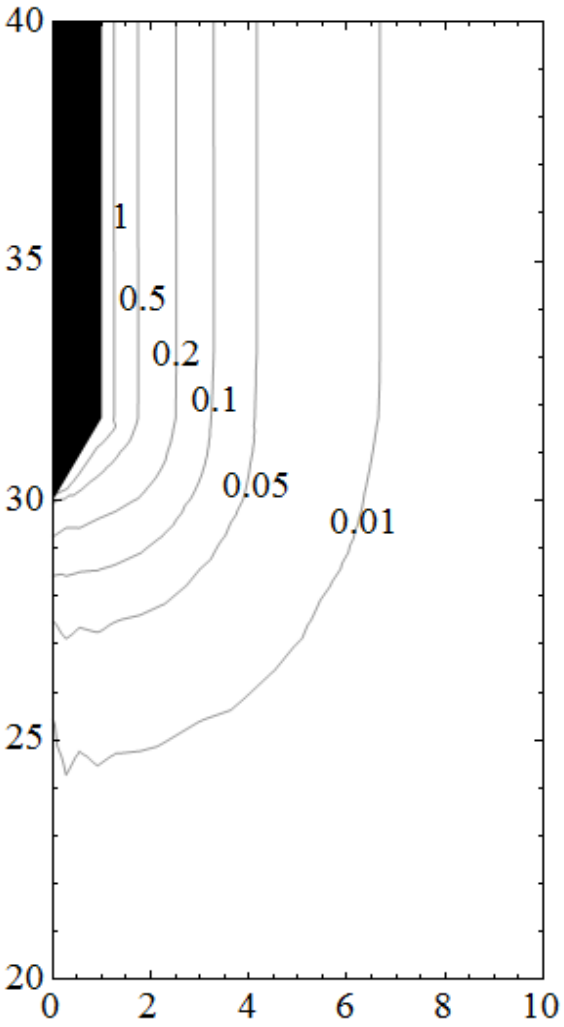

Fig. 13 Contours of the cumulative plastic deviatoric strain (I_r = 100)

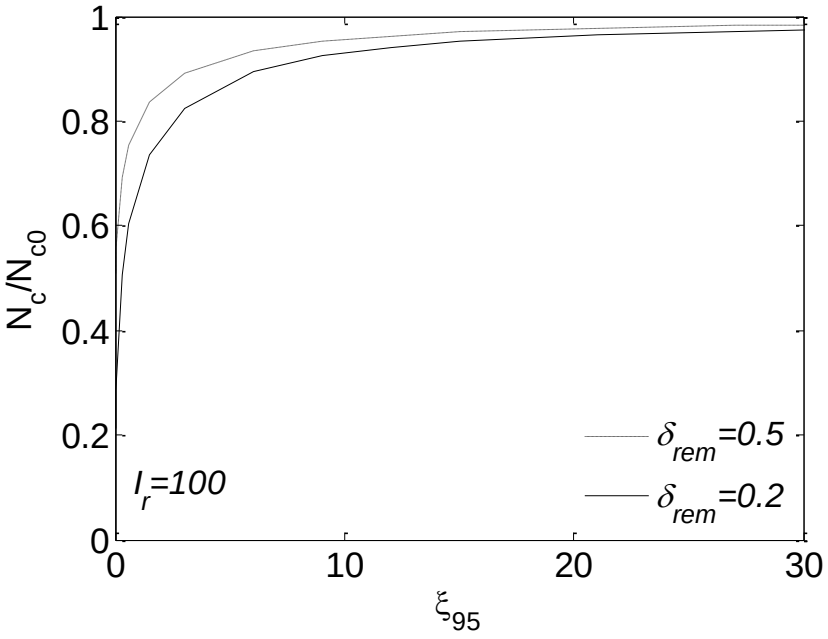

(a)

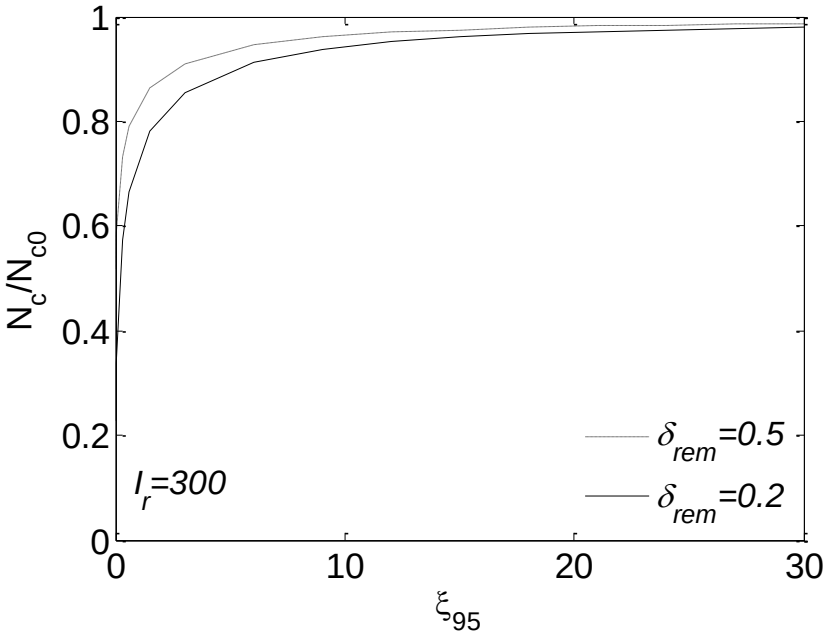

(b)

Fig. 14 Upper bound solution for the effect of strain softening on cone resistance (a) I_r = 100 (b) I_r = 300

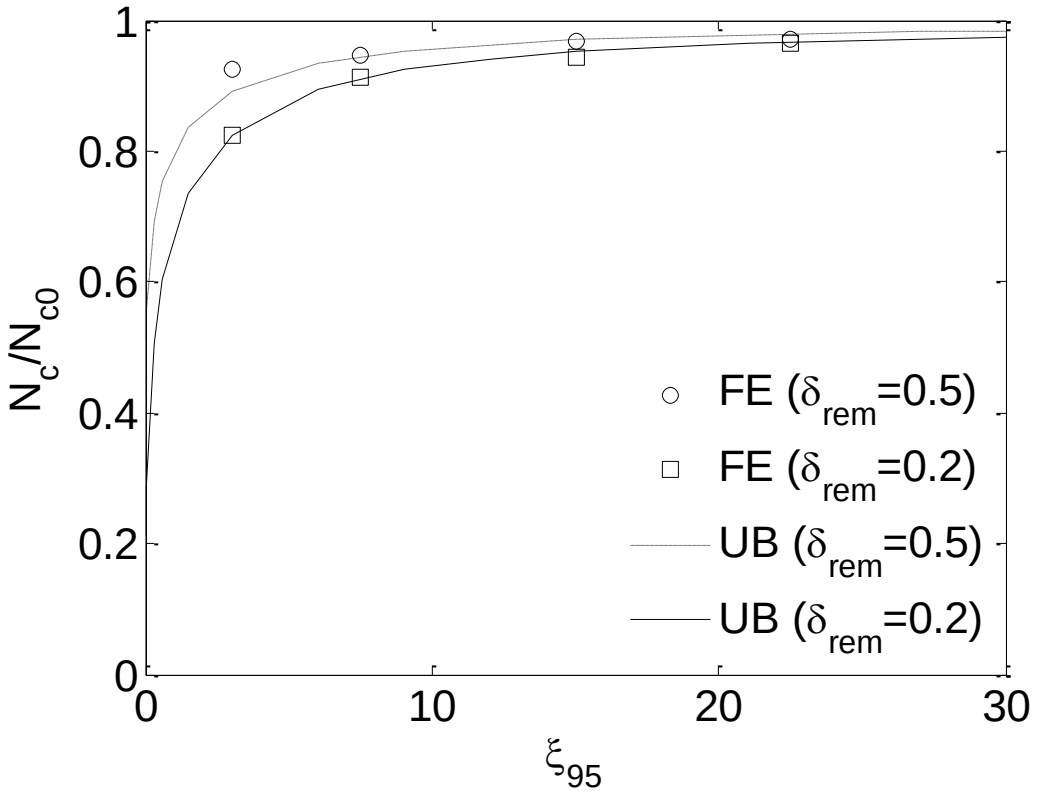

Fig. 15 Effect of strain softening on cone test: comparison between FE and UB (I_r = 100)

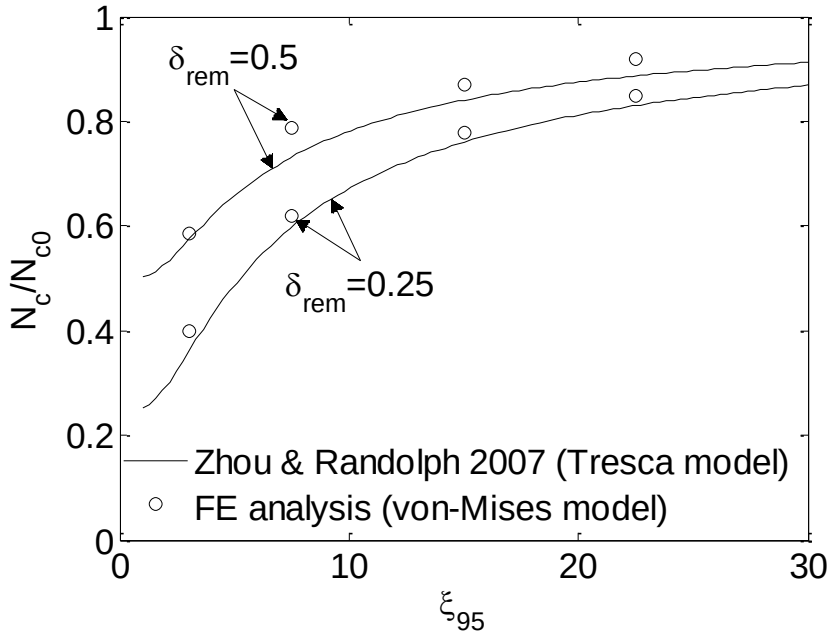

Fig. 16 Effect of strain softening on T-bar test

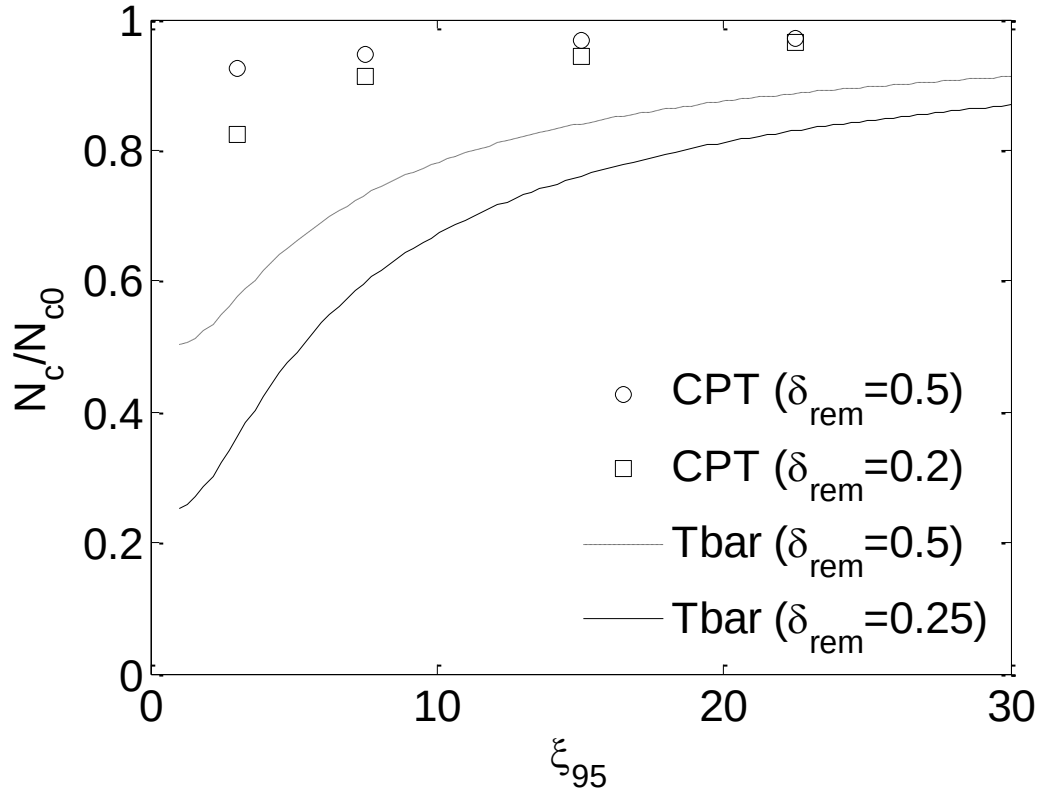

Fig. 17 Effect of strain softening on cone test: comparison between CPT and T-bar

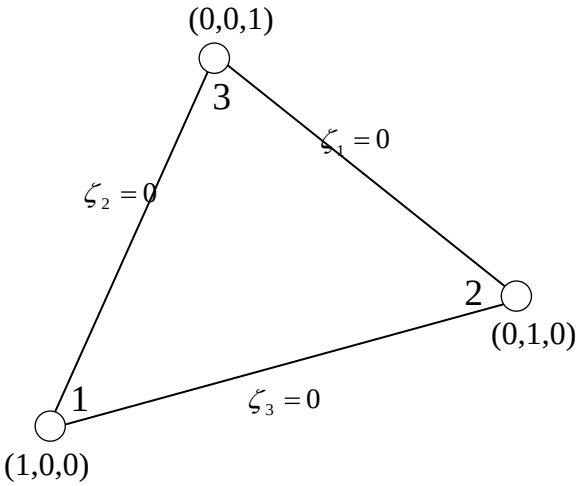

Fig.18 Triangular coordinates

Source	Correlation between I_r and bearing capacity	Numerical method used for deriving the correlation
Nazem et. al (2012)	$2.32+1.69 \ln(I_r)$	ALE
Liyanapathirana (2009)	$1.0+1.825\ln(I_r)$	ALE
Lu et al. (2004)	$3.4 + 1.6 \ln(I_r)$	RITSS
Yu et. al (2000)	$0.33+2.0 \ln(I_r)$	Steady-state FE analysis
van den Berg (1994)		Eulerian FE
Whittle (1992)	$1.51+2.0 \ln(I_r)$	Strain path finite element (approximate geometry)
Teh and Houlsby (1991)	$1.25+1.84 \ln(I_r)$	Strain path finite element

Table 1: Effect of Soil rigidity index on the cone resistance